Microporous and Mesoporous Materials 241 (2017) 185–191

Contents lists available at ScienceDirect

Microporous and Mesoporous Materials

journal homepage: www.elsevier.com/locate/micromeso

Kinetics of spontaneous liquid-gas imbibition in carbon molecular sieves used for O_2/N_2 separation

Xinyu Jia, Shaoping Xu*, Yuanyuan Cong

State Key Laboratory of Fine Chemicals, Institute of Coal Chemical Engineering, School of Chemical Engineering, Dalian University of Technology, No. 2 Linggong Road, Dalian 116024, China

ARTICLE INFO

Article history:
Received 30 August 2016
Received in revised form
26 October 2016
Accepted 31 December 2016
Available online 3 January 2017

Keywords:
Spontaneous liquid-gas imbibition
Carbon molecular sieves
Kinetics
Air separation
Micropores

ABSTRACT

The kinetics of spontaneous liquid-gas imbibition in micropores of carbon molecular sieves (CMSs) used for air separation has been investigated. Based on the kinetics, the microporous textures of CMSs could be estimated, and a new assessment method for O_2/N_2 separation performance of CMSs in pressure swing adsorption (PSA) was established. Water was chosen as the imbibition liquid probe, and N_2 and O_2 were chosen as the gas probes. The pseudo-second-order (PSO) kinetic model and the linear driving force (LDF) model were employed to confirm that the rate-limiting steps of the spontaneous water-O_2/N_2 imbibition were mainly attributable to the surface adsorption of water and the diffusion of gas through the micropore entrence or interior in CMSs. Water molecules invade into the narrower micropore mouths prior to the wider micropore mouths. An O_2/N_2 selectivity coefficient K was established to assess the air separation performance of CMSs. When the K value is equal to zero, the size distribution of micropore mouths in CMSs is the fittest for the air separation and the highest N_2 production can be obtained. But with K gradually deviating zero, the air separation performance of CMSs decreases.

1. Introduction

Carbon molecular sieves (CMSs) are porous carbons with distinguishable macropores and a great deal of micropores (size < 0.7 nm) with sharp pore size distributions [1,2]. The micropore of molecular size from either the pore mouth or the pore itself creates a barrier for the molecule diffusion [3–8]. The barrier could be the rate-limiting factor in the transport of larger molecules. Hence, CMSs show significant kinetic selectivity to the molecules with different molecular sizes. The gas uptake kinetics on CMSs is mainly controlled by either the barrier resistance at micropore mouths obeying the linear driving force (LDF) model or the diffusional resistance along the micropores following the fickian diffusion law or a combination of both described by the dual resistance model [9,10]. For a particular adsorption process, the uptake mechanism depends on the relative sizes of the micropore mouths in CMSs and the adsorbate molecules [11].

Air separation using CMSs is a kinetically controlled process depending on the differences between the uptake kinetics of O_2 and N_2. O_2 has a kinetic diameter of 0.346 nm, whereas that of N_2 is 0.364 nm. In order to be effective for the air separation in pressure swing adsorption (PSA), the CMS should own the micropores with uniform pore mouths of molecular size and relatively large pore volume to ensure a good selectivity of O_2/N_2 and a high O_2 uptake capacity. So, an accurate and simple method for the measurements of micropores in CMSs is desired [12–14]. The traditional measurement technologies, such as molecular probe techniques [15,16] that have been used for the determination of the micropore size-exclusion property of CMSs, could not distinguish whether the size-exclusion property comes from the barrier of micropore mouth or that of the micropore itself. In addition, they have the shortcoming of high cost, wasting time and complex operation.

Spontaneous liquid-gas imbibition has been applied to the assessment of the structural characteristics of mesopores and macropores by measuring the liquid diffusion amount and distance on the basis of the capillarity [17,18]. In this process, the wetting phase, i.e., the liquid, spontaneously invades into the pores medium, and the unwetting phase, i.e., the gas in the pores, is driven simultaneously. The spontaneous liquid-gas imbibition can take place in micropores as well [19,20]. However, the invasion of liquid into micropores is different from that into the larger pores [21–25]. A variety of attempts have been made on the transport of liquids through the microporous materials. They were mostly based on the

* Corresponding author.
E-mail address: huizixu@hotmail.com (S. Xu).

http://dx.doi.org/10.1016/j.micromeso.2016.12.040
1387-1811/

direct observations of the confined liquid by transmission electron microscope (TEM) [23], environmental scanning electron microscope (ESEM) and nuclear magnetic resonance (NMR) [24], or on molecular dynamics simulation [25]. These studies indicated that the properties of the fluids confined in the pores of molecular size level differ markedly from those of the bulk fluids in larger pores, and the spontaneous liquid-gas imbibition based on the capillarity is not available to the micropores.

In our laboratory, the spontaneous liquid-gas imbibition in microporous materials at ambient temperature has been studied to assess the micropores, which has been demonstrated to be a good alternative to complement N_2 adsorption at 77 K limited by diffusional problems of N_2 molecules inside the micropores [26]. Typically, the equilibriums of the process based on the liquid probes with varied molecular sizes were focused on assessing the micropore size and size-exclusion property of the microporous materials.

The present work aims to study the kinetics of spontaneous liquid-gas imbibition in micropores of CMSs used for air separation. Water has been used as the liquid probe. N_2 and O_2 have been chosen as the gas probes. The pseudo-second-order (PSO) kinetic model and linear driving force (LDF) model have been employed to describe the kinetics, and upon that the microporous textures of the CMSs have been elucidated. In addition, the kinetics has been correlated to the O_2/N_2 separation performance of CMSs in PSA.

2. Materials and methods

Eight commercial CMSs (CMS-1~CMS-8) in the form of extruded pellets with diameter 0.10–0.15 cm and length 0.25–0.3 cm were used as adsorbents in this study. All the samples have almost the same average particle diameter of about 0.12 cm, so that the difference of the influence of particle size on the liquid-gas imbibition among them could be excluded. Before imbibition test, the CMS pellets were washed three times with distilled water and then dried overnight in a drying oven at 423 K.

The spontaneous water-gas imbibition at 303.2 K was conducted with an experimental setup schematized in Fig. 1. About 1.0 g CMS pellets were firstly introduced into the sample chamber 3, and saturated with the gas at the gas flow rate of 200 ml min^{-1} for 2 h after the temperature of the apparatus reached constant. Then, about 6.0 g water was pushed from the liquid reservoir 2 into the sample chamber 3 to wet the CMS pellets, and the electromagnetic valves S4~S6 were closed immediately to ensure a sealed condition. In this case, water molecules spontaneously invaded into CMSs and gas molecules were driven simultaneously. The pressure P_t with time on-stream in the sealed system, measured by the pressure sensor 5, were recorded by the data acquisition station 8, from which the gas recovery volume could be obtained. Before the experiments, the water was saturated with the gas probe at a flow rate of 80 ml min^{-1} for 3 h to avoid the gas recovered being dissolved in the water. During the water-gas imbibition, the water in the sample chamber 3 was stirred vigorously to exclude the influence of the external diffusion of water and gas outside the CMS surface on the kinetics of the water-gas imbibition.

To obtain the kinetic curves of the gas recovery ($V_t/V_e \sim t$), the pressure values were converted to the volume V_t (ml g^{-1}) of the gas recovered by water in standard condition ($T_0 = 273.2K, P_0 = 101.325$kPa) by the equation

$$V_t = \frac{(P_t - P_{t=0})(V_s - V_l)T_0}{P_0 T} \quad (1)$$

where $P_{t=0}$ is the initial pressure (kPa) in the sample chamber 3, V_s is the volume of the sample chamber 3 (ml), V_l is the volume of the water (ml), V_t is the gas recovery volume at time t, V_e is the equilibrium gas recovery volume (ml g^{-1}), and V_t/V_e is the relative volume of the gas recovery.

The gas recovery coefficient η obtained by equation (2) was introduced to calculate the net gas recovery volume by subtracting the volume occupied by the liquid vapor in the evolved gas. P_S is the saturated vapor pressure of water at the given temperature (kPa).

$$\eta = \frac{P_0 - P_S}{P_S} \quad (2)$$

For evaluation of the microporous textures of CMSs, N_2 adsorption at 77 K was conducted in a JW-BK122W volumetric adsorption apparatus. The N_2 adsorption isotherms were analyzed by the Horvath–Kawazoe (HK) method to evaluate the micropore volume V_{mic} and micropore size D_{mic}, and by the single point BET method to obtain the total volumes V_{tot} of the samples.

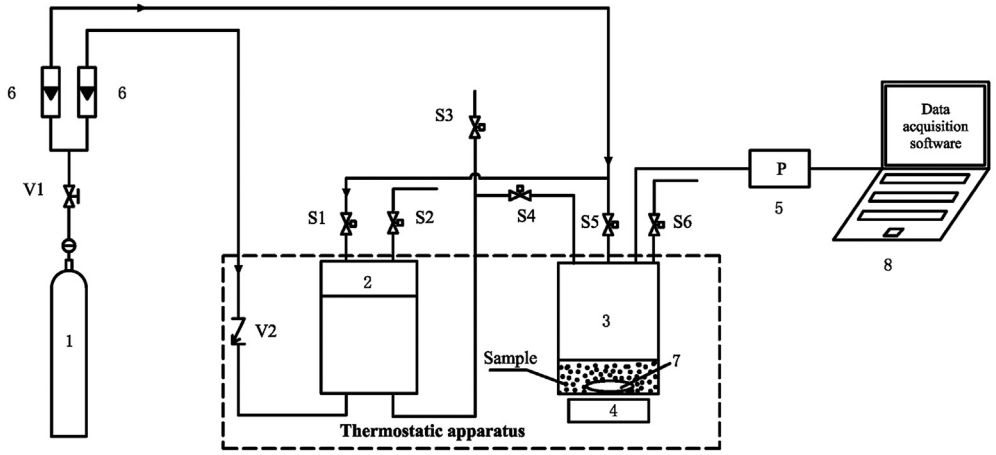

1-gas cylinder; 2-liquid reservoir; 3-sample chamber; 4-magnetic stirring apparatus;
5-pressure sensor; 6-rotor flowmeter; 7-stirring bar;
8-data acquisition station; S1~S6-electromagnetic valves

Fig. 1. Schematic diagram of experimental setup for imbibition tests.

To measure the air separation performance of CMSs in PSA, a series of PSA experiments for N_2 production from air were carried out in a two-column PSA unit packed with CMS-1~CMS-8, respectively. In a fixed PSA cycle at 303.2 K, the adsorption pressure of 0.5 MPa and the desorption pressure of 0.1 MPa were applied. The adsorption time and pressure equalization time were 64 s and 1s, respectively. At a constant flow rate of production gas with 1.0 ml min^{-1} g^{-1}, the N_2 concentrations in production gas and the capacity of N_2 per time were obtained.

3. Results and discussion

3.1. Porous texture characterization of CMSs

Table 1 shows the porous parameters of CMSs from N_2 adsorption at 77 K. For all the CMS samples, no significant N_2 adsorption could be observed, and the calculated V_{mic} and V_{mic}/V_{tot} values are very small. Hence, the N_2 adsorption at 77 K is not suitable for evaluating the micropores in CMSs because of the diffusion constriction of N_2 at such a low temperature.

In liquid state, water molecules exist as a “structural unit” of several molecules linked by hydrogen bonds. As researchers have reported by molecular dynamics simulations, in a single-walled carbon nanotube of 1.0 nm in diameter, the “unit” could be a one-dimensionally ordered chain of water molecules and spontaneously enter into the nanotube [25,27]. Its smallest diameter could be shaped in a confined space to be approximately that of a single water molecule, which is smaller than that of N_2 and O_2. Hence, the liquid water could spontaneously enter into the micropores in CMSs and replace the pre-adsorbed N_2 and O_2 fully. As a supercritical gas at 303.2 K, N_2 could diffuse into and fill the micropores of CMSs in a condensed state, whereas in the larger pores there is only a single layer of N_2 molecules [28]. The N_2 filling in micropores contributes the vast majority of the N_2 adsorbed, and the uptake volume in the condensed state would approach the micropore volume of CMSs. As shown in Table 2, for all the CMSs, the equilibrium N_2 recovery volume ($V_{e,r}$) from the spontaneous water-N_2 imbibition is a little bigger than the equilibrium N_2 uptake volume ($V_{e,a}$) from the N_2 adsorption at the same conditions. In other words, water could replace those N_2 molecules that could not be desorbed by vacuum as in the case of physical adsorption. As discussed above, it is reasonable that the equilibrium N_2 recovery volume could be a measure of the micropore volume in CMSs. Specifically in Table 2, CMS-3 presents the greatest $V_{e,r}$ value and therefore has the largest micropore volume among the eight CMSs. Table 2 also gives the equilibrium recovery volumes of O_2 from the spontaneous water-O_2 imbibition. For every CMS, the $V_{e,r}$ value of O_2 is slightly less than that of N_2. The reason may be that the boiling point of O_2 is higher than that of N_2, and so that the density of O_2 in the micropores is less than that of N_2. The biggest relative difference of the $V_{e,r}$ values between O_2 and N_2 is less than 5%, which lays a ground for comparing the gas recovery kinetics between O_2 and N_2 based on the relative recovery volume V_t/V_e.

Table 1
Porous parameters of CMSs from N_2 adsorption at 77 K.

Sample	D_{mic} (nm)	V_{mic} (ml g^{-1})	V_{tot} (ml g^{-1})	V_{mic}/V_{tot}
CMS-1	1.17	0.0010	0.023	0.0043
CMS-2	1.16	0.0013	0.021	0.0062
CMS-3	1.17	0.0015	0.031	0.0048
CMS-4	1.17	0.0015	0.023	0.0065
CMS-5	1.38	0.0012	0.020	0.0060
CMS-6	1.11	0.0013	0.018	0.0072
CMS-7	1.10	0.0014	0.015	0.0080
CMS-8	1.10	0.0012	0.014	0.0082

3.2. Kinetics of spontaneous water-gas imbibition on CMSs

3.2.1. Phenomena of the spontaneous water-gas imbibition

Fig. 2(a) and Fig. 2(b) present the kinetic curves of spontaneous water-O_2 and water-N_2 imbibition at 303.2 K on the eight CMSs, respectively. At the start of every process, the gas recovery volume increases almost linearly with time. Table 3 lists the initial gas recovery rate v_0 defined as the gas recovery volume per time (s). For both O_2 and N_2, the gas recovery rates are in the same order: CMS-1 > CMS-2 > CMS-3 > CMS-7 > CMS-4 > CMS-5 > CMS-6 > CMS-8. As discussed in Introduction, the barrier resistance at micropore mouths restricts the molecule diffusion. As the size of micropore mouth gets narrower, the barrier resistance becomes more and more strong. Hence, the average size of micropore mouths in CMSs should follow the same order as the gas recovery rates. For every CMS sample, Table 4 also presents that the water-O_2 system has the larger gas recovery rate than the water-N_2 system, meaning that the diffusion of O_2 with smaller molecular size out of micropores is faster than that of N_2. In addition, with the decrease of the micropore mouth width, the ratio of the O_2 recovery rate to that of N_2, i.e., the selectivity of O_2/N_2, increases.

3.2.2. Kinetic models for the spontaneous water-gas imbibition

The spontaneous water-gas imbibition on CMSs consists of several individual steps, i.e., the diffusion of water from the bulk fluid to the external surface and then from the pore mouth into the pores of CMSs, the adsorption of water and simultaneous desorption of the pre-adsorbed gas on the internal surface of CMSs, and the diffusion of the desorbed gas through the pores and further through the water film on the external surface of CMSs. The influence of the external diffusion of water and gas through the water film on the kinetics could be excluded by the vigorous stir of water. The gas evolution is caused by the water invasion, and the two processes carry on simultaneously. So, the rate-limiting steps in the overall process could then be attributed to the surface adsorption of water (or the desorption of the pre-adsorbed gas) and the diffusion of gas through or out of micropores in CMSs. For the characteristically nonpolar CMS samples produced in similar way and having similar surface property as is the case in this study, the kinetics of the water-gas imbibition thus depends mainly on the microporous texture.

To elucidate the kinetic mechanism of the water-gas imbibition and the microporous texture of CMSs, the pseudo-second-order (PSO) kinetic model [29–33] and the linear driving force (LDF) model [34,35] have been used to describe the kinetic curves of the gas recovery.

The PSO model used in this work is based on the assumption that the rate-limiting step is the surface adsorption of water or the desorption of the pre-adsorbed gas. It has the form

$$\frac{dV_t}{dt} = k_2(V_e - V_t)^2 \tag{3}$$

Where k_2 is the PSO rate constant (ml g^{-1} s^{-1}), V_e is the gas recovery volume at equilibrium (ml g^{-1}), and V_t is the volume of gas recovery at time t (ml g^{-1}).

Integrating Eq. (3) and applying the initial conditions, we have

$$\frac{t}{V_t/V_e} = \frac{1}{k_2 V_e} + t \tag{4}$$

On the other hand, Eq. (4) can be rewritten as

Table 2
The equilibrium gas recovery volume $V_{e,r}$ (ml g^{-1}) and the equilibrium adsorption volume $V_{e,a}$ (ml g^{-1}) at 303.2 K and 100 kPa on different CMSss.

Sample		CMS-1	CMS-2	CMS-3	CMS-4	CMS-5	CMS-6	CMS-7	CMS-8
N_2	$V_{e,r}$	5.48	5.22	7.17	5.87	6.06	5.78	6.26	5.12
	$V_{e,a}$	5.36	5.11	7.07	5.78	5.88	5.57	6.02	4.90
O_2	$V_{e,r}$	5.34	5.12	6.92	5.35	5.87	5.34	6.09	4.92

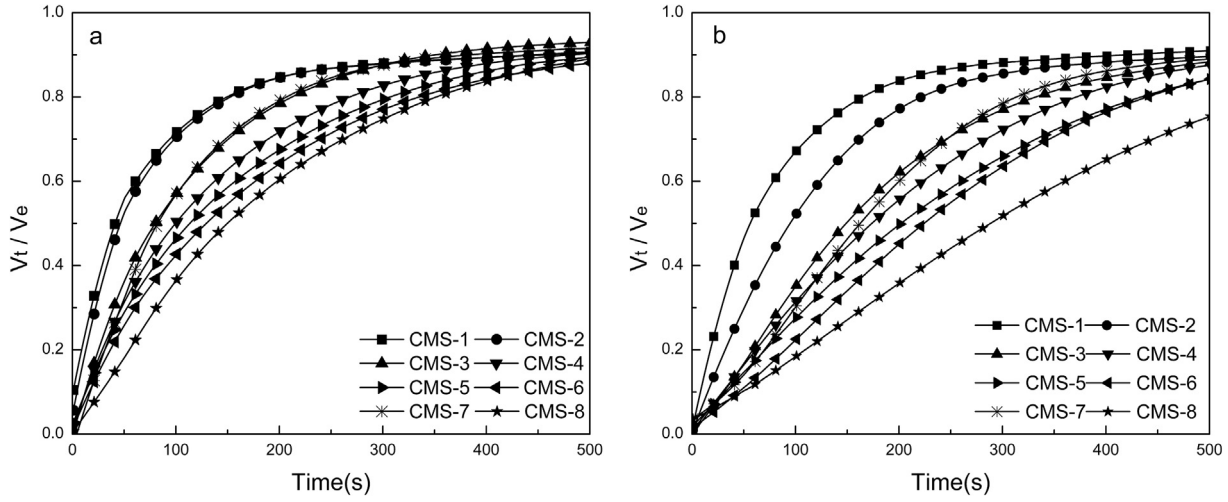

Fig. 2. Gas recovery curves of spontaneous water-gas imbibition at 303.2 K on CMSs (a-O_2, b-N_2).

Table 3
The initial gas recovery rates (s^{-1}) for O_2 and N_2 on CMSs at 303.2 K.

Sample	CMS-1	CMS-2	CMS-3	CMS-4	CMS-5	CMS-6	CMS-7	CMS-8
v_{o,N_2}	0.0119	0.0074	0.0036	0.0030	0.0027	0.0023	0.0032	0.0016
v_{o,O_2}	0.0221	0.0154	0.0078	0.0064	0.0059	0.0052	0.0068	0.0047
$v_{o,O_2}/v_{o,N_2}$	1.857	2.088	2.166	2.133	2.185	2.260	2.125	2.937

Table 4
Kinetic parameters and correlation coefficients R^2 of the PSO and LDF models for the spontaneous water-O_2 imbibition at 303.2 K on eight CMSs.

Sample	CMS-1	CMS-2	CMS-3	CMS-4	CMS-5	CMS-6	CMS-7	CMS-8
$t_{0.5}$(s)	34.99	38.54	85.66	110.63	129.15	151.02	92.01	218.35
$k_2V_e(s^{-1})$	2.86E-02	2.59E-02	1.17E-02	9.04E-03	7.74E-03	6.62E-03	1.09E-02	4.58E-03
$R^2_{(PSO)}$	0.9996	0.9992	0.9970	0.9981	0.9993	0.9988	0.9854	0.9668
$k/10^3(s^{-1})$	6.62	6.23	6.12	5.41	5.01	4.66	6.12	4.53
$R^2_{(LDF)}$	0.9331	0.9360	0.9852	0.9901	0.9945	0.9961	0.9772	0.9998

$$t = \frac{V_t/V_e}{1 - V_t/V_e}\frac{1}{k_2V_e} \tag{5}$$

At the half-life of the gas recovery process (i.e., $t = t_{0.5}$), we have $V_t = 0.5V_e$ and

$$t_{0.5} = \frac{1}{k_2V_e} \tag{6}$$

The proportionality constant k_2V_e (s^{-1}) in Eq. (4) can be defined as the 2nd-order rate index obtained from the intercept in the plot of t/V_t vs. t. It is evident that k_2V_e is the only parameter of Eq. (6), and the value is equal to the inverse of the half-life of the process. Eq. (5) shows that an increase of the k_2V_e value produces the contraction of the imbibition time. Hence, k_2V_e can be used to describe the average rate of the spontaneous imbibition.

The linear driving force (LDF) model is based on the assumption that the diffusion of gas through the barrier at the micropore entrance is the rate-limiting step in the spontaneous water-gas imbibition. It is described by the equation

$$V_t/V_e = 1 - e^{-kt} \tag{7}$$

Eq. (7) can be rewritten as

$$\ln(1 - V_t/V_e) = -kt \tag{8}$$

where the rate constant k (s^{-1}) can be obtained from the plot of $\ln(1 - V_t/V_e)$ versus time which is linear passing through the origin with a gradient equal to the k value. k can also describe the average gas recovery rate.

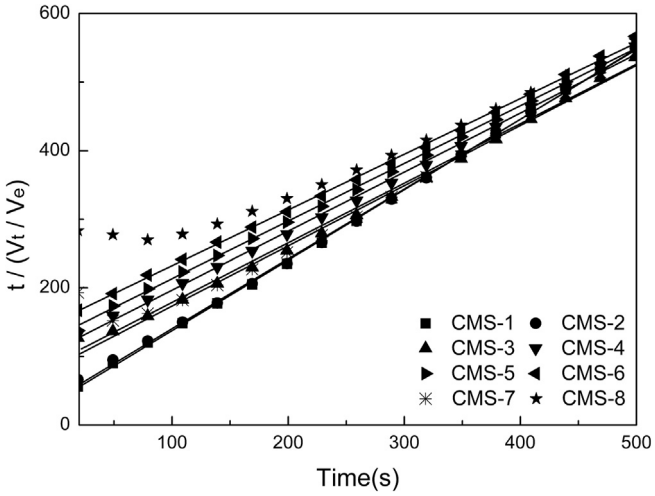

Fig. 3. Variation of $t/(V_t/V_e)$ against time for spontaneous water-O_2 imbibition at 303.2 K on CMS-1~CMS-8 with the calculated profile (–) from the PSO model.

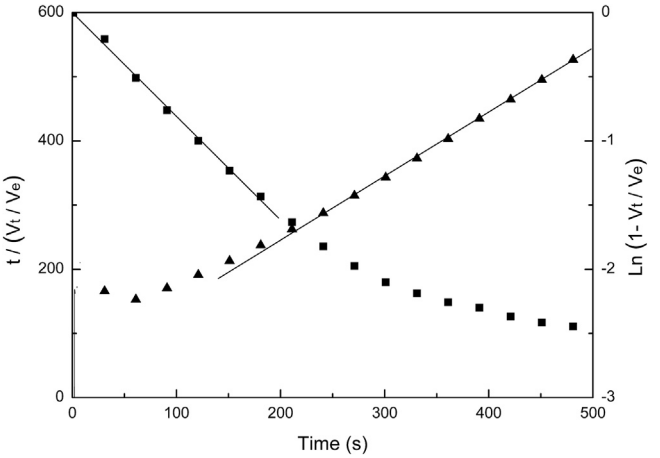

Fig. 5. Application of the PSO and LDF models to describe the spontaneous water-O_2 imbibition at 303.2 K on CMS-7.

3.2.3. *Kinetics of the spontaneous water-O_2 imbibition on CMSs*

The kinetics of the spontaneous water-O_2 imbibition on CMSs have been studied using the PSO and LDF models. The fitting results are given in Fig. 3 and Fig. 4, respectively. It can be seen that the kinetic behaviors of the water-O_2 system on different CMSs differ greatly.

On sample CMS-1~CMS-6, the graphs of $t/(V_t/V_e)$ with time according to Eq. (4) are linear, whereas the graphs of $\ln(1 - V_t/V_e)$ with time according to Eq. (8) are only linear at the initial stage followed by the increasing deviation upward from the linearity from CMS-6 to CMS-1. Therefore, all the kinetic curves are fitted to the PSO model and the surface adsorption of water is the rate-limiting step in the entire system. For the sample CMS-8, on the contrary, the graphs of $\ln(1 - V_t/V_e)$ with time are linear completely, upon that the diffusion of O_2 out of the micropore mouths controls the O_2 recovery rate and CMS-8 has the narrowest micropore mouths to restrict the O_2 diffusion.

For the sample CMS-7, neither of the two models can describe the entire water-O_2 imbibition system exactly. As can be seen in Fig. 5, the kinetics obeys the LDF model up to 200s, but over 200s it follows the PSO model. Thus, the surface adsorption of water plays a leading role in controlling the O_2 recovery rate up to 200s, but then its place is taken by the diffusion of O_2 out of the micropores. It can be concluded that CMS-7 has the far lower size uniformity of micropore mouths than other CMSs.

Table 4 shows the kinetic parameters and the correlation coefficients R^2 obtained from the two models. Both the k_2V_e values of the PSO model and the k values of the LDF model are following: CMS-1 > CMS-2 > CMS-3 > CMS-7 > CMS-4 > CMS-5 > CMS-6 > CMS-8, demonstrating that the average O_2 recovery rates and the average sizes of the micropore mouths in CMSs are following the same order, in good agreement with the statement above.

3.2.4. *Kinetics of the spontaneous water-N_2 imbibition on CMSs*

The kinetics of the spontaneous water-N_2 imbibition on eight CMSs were studied by the PSO and LDF models as well, and the fitting results are shown in Fig. 6 and Fig. 7, respectively. The kinetic parameters and correlation coefficients R^2 obtained are listed in Table 5. On the same CMS, compared with O_2, the N_2 recovery fits

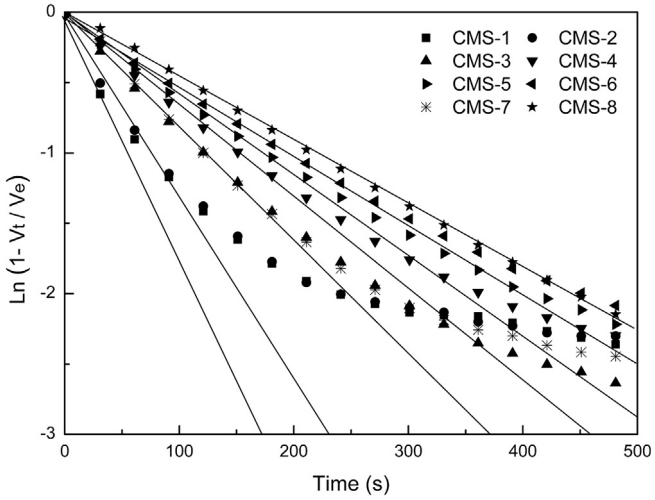

Fig. 4. Variation of $\ln(1 - V_t/V_e)$ against time for spontaneous water-O_2 imbibition on CMS-1~CMS-8.

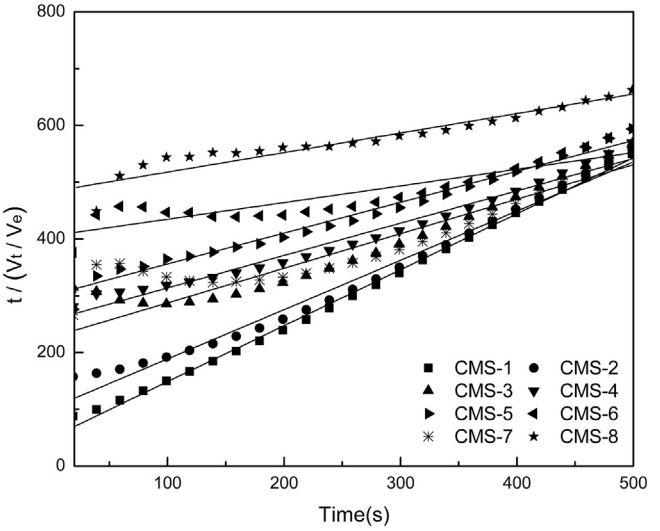

Fig. 6. Variation of $t/(V_t/V_e)$ against time for spontaneous water-N_2 imbibition at 303.2 K on CMS-1~CMS-8 with the linear regression (–) for the PSO model.

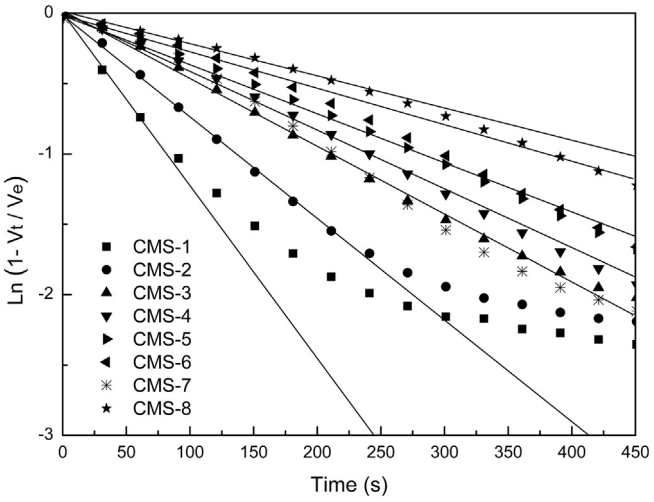

Fig. 7. Variation of $\ln(1 - V_t/V_e)$ against time for spontaneous water-N_2 imbibition at 303.2 K on CMS-1~CMS-8 with the linear regression (–) for the LDF model.

the LDF model better, because of the greater barrier resistance at the micropore mouths.

It is evident that the kinetic behaviors of the water-N_2 system on CMS-1 and CMS-2 are similar as that of the water-O_2 system. In this case, N_2 molecules are negligibly impeded by the barrier at micropore mouths, and the surface adsorption of water plays a key role as a rate-controlled step in the process. For CMS-3~CMS-5, the good linearized plots of $\ln(1 - V_t/V_e)$ vs. time have demonstrated the validity of the LDF model. That is, the micropore mouths are narrow enough to confine the transport of N_2 molecules, and the diffusion of N_2 out of micropores controls the entire system. Possessing the narrower micropore mouths, CMS-6 ~ CMS-8 should have displayed a better fitting to the LDF model than CMS-3 ~ CMS-5. However, their graphs shown in Fig. 7 are only linear at the initial stage and then deviate downward from the linearity, opposite from that of CMS-1 and CMS-2. And they have poorer linear relationships for the plots of $t/(V_t/V_e)$ vs. time in the PSO model than other CMSs by the comparison of the R^2 values. Hence, the water-N_2 system is controlled by not only the diffusion of N_2 through and out of the micropore mouths, but also that in the micropores of CMSs.

Through the study of the kinetics of the spontaneous water-N_2 and water-O_2 imbibition, it can be summarized that the rate-limiting steps could be attributed to the surface adsorption of water (i.e. the desorption of the pre-adsorbed gas) and the diffusion of gas through or out of the micropores. Water molecules invade into the micropores with narrower pore mouths prior to the wider pore mouths, and the water-N_2/O_2 system should be divided into two stages according to the rate-limiting factors. At the initial stage, the water molecules invade into the micropores with narrower pore mouths, where the barrier resistance can be the rate limiting factor in the transport of gas molecules. At the latter stage, water molecules gradually enter into the micropores with wider pore mouths following the micropores with narrower pore mouths being water-filled, and gas molecules are negligibly impeded by the barrier at micropore mouths, resulting in the kinetics of the process being mainly controlled by the surface adsorption of water. The latter stage grows longer and longer with the increase of the size of micropore mouths. For a particular process, the rate-limiting steps depend on the relative sizes of micropore mouths and gas molecules. Hence, the kinetics of the water-gas imbibition could be used to evaluate the relative size of micropore mouths in CMSs.

3.2.5. Assessment of the O_2/N_2 separation ability of CMSs in PSA

To obtain high N_2 production from air separation in PSA, CMSs must own the proper size of micropore mouths to guarantee not only high selectivity of O_2/N_2 but also high adsorption rates of O_2, and a relatively high micropore volume to confer high O_2 uptake capacity.

In this work, an O_2/N_2 selectivity coefficient K was introduced from the kinetics of gas recovery to assess the O_2/N_2 separation ability of CMSs in PSA. It is defined as:

$$K = \left(\frac{R^2_{(O_2,PSO)}}{R^2_{(N_2,LDF)}} - 1\right) \times 100\% \quad (9)$$

where $R^2_{(O_2,PSO)}$ is the correlation coefficient of the PSO model for the water-O_2 imbibition system, and $R^2_{(N_2,LDF)}$ is the correlation coefficient of the LDF model for the water-N_2 system. The K value can reflect the relative size of micropore mouths in CMSs.

It is expected that, when the K value is equal to zero, the sample CMS should have the most fitted micropore texture for producing N_2 from air separation in PSA. In this case, the water-O_2 imbibition system is mainly controlled by the surface adsorption of water, and the water-N_2 system is controlled by the diffusion of N_2 out of the micropore mouths. The barrier resistance at the micropore mouths to N_2 is far stronger than that to O_2, and the sample CMS can adsorb O_2 over N_2 selectively and sufficiently. However, when the K value is much larger than zero, the micropore mouths are too wide to have any appreciable selectivities of O_2/N_2. Conversely, When K is far less than zero, the micropore mouths are too narrow to adsorb O_2 sufficiently within a short adsorption time. Despite the excellent selectivity of O_2/N_2 caused by the molecular size of N_2 close to the average micropore mouth size, the productivity of N_2 is much lower.

The O_2/N_2 separation ability of the eight CMSs were assessed by this method. Table 6 lists the O_2/N_2 selectivity coefficient K values of the eight CMSs. They are in the order: CMS-1 > CMS-2 > CMS-3 ≈ CMS-4 > 0 > CMS-5 > CMS-6 > CMS-7 > CMS-8, and correspondingly the air separation performance should follow CMS-1 < CMS-2 < CMS-3 ≈ CMS-4 ≈ CMS-5 > CMS-6 > CMS-7 > CMS-8. Obviously, the sample CMS-3~CMS-5 have the highest N_2 purity in production gas, because the K values are the closest to zero. The micropore volume of CMS-3 is the largest obtained in Section 3.1. Therefore, the sample CMS-3 is the favorite adsorbent for producing N_2 from air in PSA.

Table 5
Kinetic parameters and correlation coefficients R^2 of the PSO and LDF models for the spontaneous water-N_2 imbibition on eight CMSs at 303.2 K.

Sample	CMS-1	CMS-2	CMS-3	CMS-4	CMS-5	CMS-6	CMS-7	CMS-8
$t_{0.5}$(s)	49.50	102.50	228.29	257.06	300.63	404.27	273.30	479.26
k_2V_e(s^{-1})	2.02E-02	9.76E-03	4.38E-03	3.89E-03	3.33E-03	2.47E-03	3.65 E−03	2.09E-03
$R^2_{(PSO)}$	0.9980	0.9860	0.9158	0.9754	0.9855	0.8037	0.8061	0.7834
k/10^3(s^{-1})	6.26	5.63	4.64	4.24	3.63	3.49	4.80	2.57
$R^2_{(LDF)}$	0.9492	0.9753	0.9980	0.9993	0.9991	0.9945	0.9961	0.9946

Table 6
The O_2/N_2 selectivity coefficient K and N_2 concentration and productivity by PSA on CMSs.

Sample	CMS-1	CMS-2	CMS-3	CMS-4	CMS-5	CMS-6	CMS-7	CMS-8
K(%)	5.304	2.445	0.097	0.117	−0.016	−0.428	−1.076	−2.792
N_2(vol%)	96.5	98.9	99.4	98.1	99.2	98.9	98.0	95.3
N_2(ml min^{-1} g^{-1})	0.96	0.99	0.99	0.98	0.99	0.99	0.98	0.95

The N_2 concentration of production gas in PSA presented in Table 6 are in the order: CMS-1 < CMS-2 < CMS-3 ≈ CMS-5 > CMS-6 > CMS-4 > CMS-7 > CMS-8, in good accordance with the results of the new assessment method except for CMS-4. The reason should be further elucidated and the assessment method should be modified based on larger sample test.

4. Conclusions

The kinetics of spontaneous water-O_2 and water-N_2 imbibition in CMSs have been studied. Both theory analysis and experimental results demonstrate that the kinetics of the water-gas imbibition on CMSs is mainly controlled by the surface adsorption of water, and the diffusion of gas along the micropores or through the barrier at the pore mouths. In a particular process, the rate-controlled steps depend on the relative sizes of micropore mouths and gas molecules. The water invasion takes place in the micropores with narrower pore mouths prior to wider pore mouths. Through the wider micropore mouths, where the gas molecules are negligibly impeded by the barrier, the kinetics is mainly decided by the surface adsorption of water; in the transport of gas molecules into the narrower micropore mouths, the barrier resistance can be the rate-controlled step. Hence, the kinetics of the water-gas imbibition can be used to evaluate the size of micropore mouths in CMSs.

In addition, an assessment method for the O_2/N_2 separation performance of CMSs in PSA was established by introducing an O_2/N_2 selectivity coefficient K from the kinetics of the water-O_2/N_2 imbibition. When K is equal to zero, the CMS owns the most appropriate size of micropore mouths to adsorb O_2 over N_2, and with K gradually deviating zero, the O_2/N_2 separation ability reduces. The spontaneous liquid-gas imbibition method is a simple and useful tool to assess the micropores and the O_2/N_2 separation ability of CMSs in PSA.

Acknowledgements

This work is supported by the National Natural Science Foundation of China (21376046).

References

[1] D. Li, C. Li, Y. Tian, L. Kong, L. Liu, Mater. Lett. 141 (2015) 340–343.
[2] A. Shahtalebi, A.H. Farmahini, P. Shukla, S.K. Bhatia, Carbon N. Y. 77 (2014) 560–576.
[3] A. Berenguer-Murcia, A.J. Fletcher, J. García-Martínez, D. Cazorla-Amorós, A. Linares-Solano, K.M. Thomas, J. Phys. Chem. B 107 (2003) 1012–1020.
[4] H. Chagger, F. Ndaji, M. Sykes, K. Thomas, Carbon N. Y. 33 (1995) 1405–1411.
[5] A. Jayaraman, A.S. Chiao, J. Padin, R.T. Yang, C.L. Munson, Sep. Sci. Technol. 37 (2002) 2505–2528.
[6] D. Lozano-Castello, J. Alcaniz-Monge, D. Cazorla-Amorós, A. Linares-Solano, W. Zhu, F. Kapteijn, J.A. Moulijn, Carbon N. Y. 43 (2005) 1643–1651.
[7] N.A. Seaton, S.P. Friedman, J.M.D. MacElroy, B.J. Murphy, Langmuir 13 (1997) 1199–1204.
[8] Y. Yang, A.M. Ribeiro, P. Li, J. Yu, A.E. Rodrigues, Ind. Eng. Chem. Res. 53 (2014) 16840–16850.
[9] C.R. Reid, K.M. Thomas, J. Phys. Chem. B 105 (2001) 10619–10629.
[10] R.M. Rynders, M.B. Rao, S. Sircar, AIChE J. 43 (1997) 2456–2470.
[11] M. Bulow, Z. Fur Chem. 25 (1985) 81–88.
[12] A. Kapoor, R.T. Yang, Chem. Eng. Sci. 44 (1989) 1723–1733.
[13] Y. Kawabuchi, S. Kawano, I. Mochida, Carbon N. Y. 34 (1996) 711–717.
[14] S.W. Rutherford, C. Nguyen, J.E. Coons, D.D. Do, Langmuir 19 (2003) 8335–8342.
[15] Z. Hu, N. Maes, E.F. Vansant, J. Porous Mater. 2 (1995) 19–23.
[16] S. Villar-Rodil, R. Denoyel, J. Rouquerol, A. Martínez-Alonso, J.M.D. Tascón, Thermochim. Acta (2004) 141–144.
[17] E. Senbetta, C.F. Scholer, J. Am. Concr. Inst. 81 (1984) 82–86.
[18] T.C. Powers, J. Am. Ceram. Soc. 41 (1958) 1–6.
[19] F.B. Aarden, P.J.A.M. Kerkhof, A.J.J. van der Zanden, AIChE J. 45 (1999) 268–275.
[20] A. Borhan, K.K. Rugnta, J. Colloid Interface Sci. 58 (1993) 403–411.
[21] R.K. Harris, T.V. Thompson, P. Forshaw, N. Foley, K.M. Thomas, P.R. Norman, C. Pottage, Carbon N. Y. 34 (1996) 1275–1279.
[22] J. Maran Di Leo, J. Maran, J. Mol. Struct. 623 (2003) 159–166.
[23] A.L. Yarin, A.G. Yazicioglu, C.M. Megaridis, M.P. Rossi, Y. Gogotsi, J. Appl. Phys. 97 (2005).
[24] L.M. Dickinson, R.K. Harris, J.A. Shaw, M. Chinn, P.R. Norman, Magn. Reson. Chem. 38 (2000) 918–924.
[25] G. Hummer, J.C. Rasaiah, J.P. Noworyta, Nature 414 (2001) 188–190.
[26] Y. Su, S. Xu, J. Wang, R. Xiao, J. Colloid Interface Sci. 377 (2012) 416–420.
[27] J. Zheng, E.M. Lennon, H. Tsao, Y. Sheng, S. Jiang, J. Chem. Phys. (2005) 1–7.
[28] D.D. Do, H.D. Do, Carbon N. Y. 41 (2003) 1777–1791.
[29] Y. Ho, G. McKay, J. Environ. Sci. Heal. Part A 34 (1999) 1179–1204.
[30] Y. Ho, G. McKay, Process Biochem. 34 (1999) 451–465.
[31] S. Azizian, J. Colloid Interface Sci. 276 (2004) 47–52.
[32] Y.S. Ho, J. Hazard. Mater. 136 (2006) 681–689.
[33] F.C. Wu, R.L. Tseng, S.C. Huang, R.S. Juang, Chem. Eng. J. 151 (2009) 1–9.
[34] M.B. Rao, R.G. Jenkins, W.A. Steele, Langmuir 1 (1985) 137–141.
[35] C.R. Reid, K.M. Thomas, Langmuir 15 (1999) 3206–3218.